

Evaluation of the Rosetta Coastal Zone through Integration of Remote Sensing and Statistical Analysis (DSAS)

WALEED FOUAD, ALI MASRIA, KARIM NASSAR, MOHAMED TAREK SHAMAA

Abstract— Rosetta promontory in Egypt is liable to coastal problems such as severe erosion beside the shoreline and siltation problem at the outlet. This problem is due to many reasons including the lack of water and sediment resources as a side effect of constructing the High Aswan Dam (HAD) and other head structures along the Nile River. Remarkably, the situation is still unstable although protection works have been constructed to mitigate shoreline erosion. The main goal of our study is to analyze the coastal region at Rosetta promontory and to determine erosion and accretion rates besides accretion/erosion patterns through using the integration between remote sensing techniques and statistical analysis of shoreline using DSAS software. Moreover, it aims to determine the hotspot areas that need to be protected. Ultimately, a decision matrix will be developed to indicate the level of vulnerability along the shoreline; accordingly, the decision-makers will have a powerful tool to help them make decisions regarding coastal zone management.

Index Terms— Rosetta Coastal Zone, Remote sensing and GIS, DSAS, Shoreline change, Shoreline prediction.

1 INTRODUCTION

Several international studies included quality and quantity analyses of Spatio-temporal shoreline variations (Addo & Kufogbe, 2011; Kabuth et al., 2013; Thi et al., 2014; El-Sharnoby et al., 2015; Murali et al., 2015; El-sharnouby et al., 2015; Masria et al., 2015; Nandi et al., 2016; Anand et al., 2016; Kermani et al., 2016; Nassar, Fath, et al. 2018; Nassar, Mahmud, Masria, et al. 2018; Nassar, Mahmud, Fath, et al. 2018).

The Rosetta promontory is a regional example of a variety of outlets that are impacted by many coastal issues, such as coastal erosion. That is because the Nile River lacks water and sediment supplies to the detriment of constructing infrastructure for flood protection along the River Nile (Frihy 2001). Furthermore, the Rosetta outlet is used as an offshore drain for eroded sediments from Abu Quir Bay and Rosetta (Ahmed 2006). Such sediments build up at the exit and cause major problems with the navigation, livelihoods in the region and also threaten the surrounding area with flooding, as this diminishes the waterway capacity.

While protection works were built to minimize erosion in the outlet Rosetta (two defences 5 km long and 14 east and west of the promontory) as stated by Fanos, Khafagy, et al. (1995). In EL-Sayed et al. (2005), there is still an unstable coastline along the Rosetta promontory, which has not been suffi-

ciently effective to avoid it. Coastal infrastructure minimized the issue of erosion within the building area, but had a negative effect in the vicinity.

The main purpose of the current study is to examine the Rosetta promontory coastal area and evaluate the erosion and accretion levels and the protected areas. Moreover, this study is specifically designed to (1) identify erosion/accretion patterns across coastal areas and detect the change in the land cover up to the period 1984-2019; (2) evaluate the development of land use near the coast; (3) track change in the shoreline at different periods (1984-2019); (4) determine coastal change levels using DSAS, and (5) forecast shoreline changes up to 2100.

2 STUDY AREA

Rosetta Promontory is considered one of the most vulnerable areas along the Nile Delta coastal area. It lies on the north-western Nile Delta coast as stated in Fig. 1a. This promontory is one of the most important areas since it is used for transportation, agriculture, and fishing activities. Frihy et al. (1994) state that the promontory is a coastal headland with flat terrain covered by sand mounds and small sand dunes. They also emphasize that the beach is composed of fine to very fine quartz sand and rich in heavy minerals. There are also many low-lying areas forming salt-crusted sabkhas. The headland is inundated periodically by seawater during winter storm surge. Agricultural lands encompass the River Nile course. Also, Badr et al. (2005) indicate that the dynamic factors that influence the shape of the Nile Delta coast are the same as those found in other deltas. They add that most of the energy driving nearshore processes along the delta coast come from the Mediterranean Sea in the form of wind, waves, currents, and sea-level variation. Moreover, the direction and strength of wind play a vital role in controlling the processes that form the inland coastal areas. As shown in Fig. 1b, the annual wind

- Waleed Fouad is currently pursuing a master's degree program in environmental engineering at Mansoura University, Egypt, PH-+20 122 408 2002.
- Ali Masria is currently a lecturer at Jouf University, Saudi Arabia, PH-+966 56 919 0483. E-mail: ali_masria@yahoo.com
- Karim Nassar is currently a lecturer at Mansoura University, Egypt, PH-+201098118002. E-mail: karim.nassar@ejust.edu.eg
- Mohamed Tarek Shamaa is currently an associate professor at Mansoura University, Egypt, PH- +20 109 695 3045.

rose offshore the Nile Delta coast indicates that the wind is predominantly blowing from the North West (NW) and West North West (WNW) directions. Speeds average 3-5 m/s in summer and spring seasons and 5-7 m/s in the winter season, from NW direction.

According to waves, the obtained data during the period from 1985 to 1990 show that the maximum significant wave height and wave period at Abu-Quir are 5.5 m and 13 sec. Badr et al. (2005) state that these wave data have been subjected to statistical analysis in order to get the percentage of occurrence of certain wave height from a certain direction, known by the wave rose. This wave rose indicates that the predominant wave directions are from WNW, NNW, N, and W with a small portion of waves arrived from the NNE and NE especially in March and April.

Badr et al. (2005) also mentioned that coastal current is seen as a significant factor in the shipping of sediment along

the coast or on / offshore. In addition, the surfing zone and offshore zone are being combined. This current will also be reversed within a few months, depending on the wind direction and bottom morphology (April, May, and/or August on the east, May, July, November and/or December on the west side).

The water level changes are reported near the headland of Rosetta between 1995 and 2000. The collected data were analysed and thus the tide in the area was found to be semi-diurnal. It is also noted that the maximum recorded water level was around 80 cm and the lowest water level was -64 cm. The data from the Institute of Coastal Research (Institutes of Coastal Research of Alexandria) revealed a land shrinkage of about 0.163 cm/year (from 1951 to 1988) in Alexandria, 1.0 mm / year in Burullus (Fanos 2001),(Stanley & Warne 1993), (Sharaf El-Din et al. 1989).

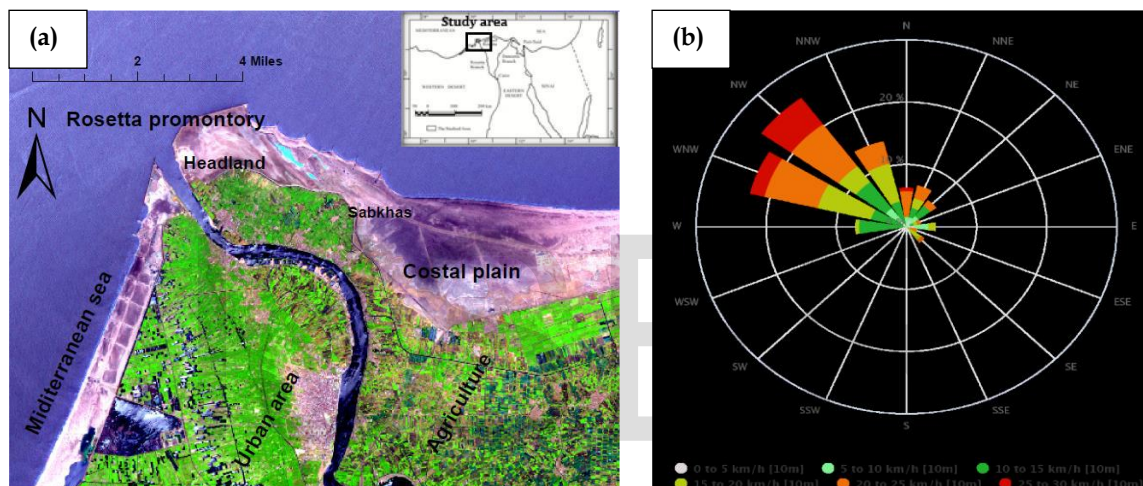


Fig. 1. (a) Rosetta promontory at the terminal of the Rosetta branch, SPOT image 2012, (b) the qualitative wind/wave rose.

3 MATERIALS AND METHODS

3.1 Sources of Data

The image data was taken for 35 years at inconsistent times spanning from 1984 until 2019. Of note, the images were created in good quality without successful clouds almost in the

summer. Three images from Landsat 4-5 (30 m spatial resolution) took in 1984, 1995, 2004, 2011, and one from Landsat 08 (30 m spatial resolution) taken in 2019 were taken in Table 1. For ENVI version 4.8, all image scenes were subjected to image processing. We used the following website to download satellite images: <https://earthexplorer.usgs.gov/>.

TABLE 1
THE IMAGES OF SATELLITE USED IN THE STUDY

Acquired Data	Spacecraft ID/Sensor	Pixel Size (m)	Used bands
25/07/1984	Landsat_4-5	30	1,2,3
22/06/1995	Landsat_4-5	30	1,2,3
14/06/2004	Landsat_4-5	30	1,2,3
25/04/2011	Landsat_4-5	30	1,2,3
10/07/2019	Landsat_08	30	2,3,4

3.2 Classification of images

The classification method was designed to distinguish the land cover units so that identification could be modified for each type. All spectral bands (1984, 1995, 2004, 2011, 2019) within TM and ETM images were used for this classification except for

those in the thermal bands. Pre-classification images are displayed in Fig. 3.

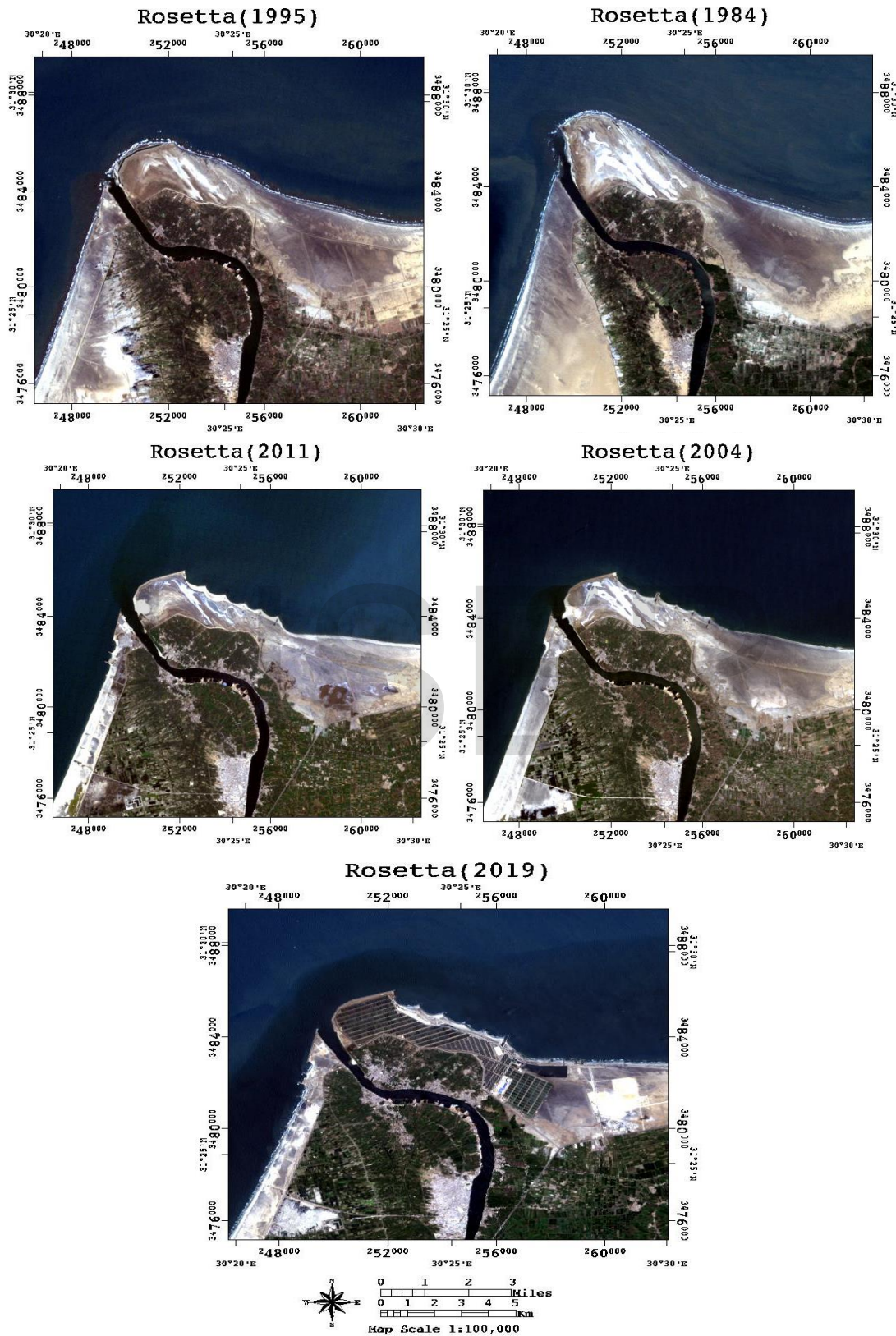


Fig. 3 original images before classification for different dates (1984, 1995, 2004, 2011 and 2019)

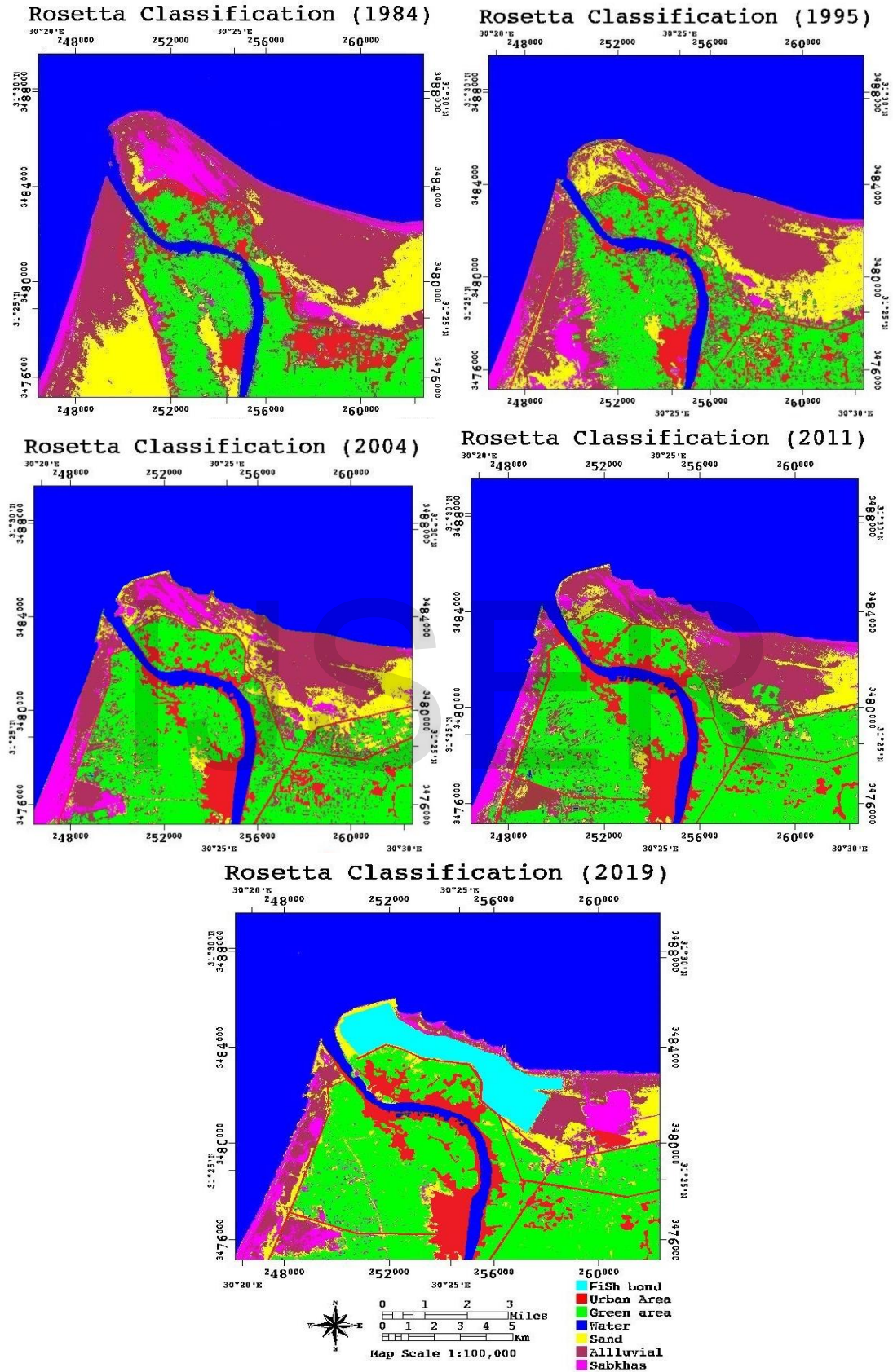


Fig. 4. The Landuse/Landcover supervised-classification for the Landsat images in 1984, 1995,2004, 2011, and 2019.

In order to divide these three images into seven land cover groups including water, urban area, green area, Sabkhas (salt-flate), and alluvial zones, the supervised classification by supporting vector machine algorithms was made. Instead, a 3x3 majority/minority technique was used to refinish classified images to eliminate odd pixels in the classified matrix and minimize noise on the display maps.

The accuracy assessment of all land cover maps ranged from (0.97-1.0) for both the producer and user accuracies as well as for the overall accuracy. The areas were computed for each land cover type in each classified image shown in Fig. 4. Table 2 indicates the descriptions of the land cover types used

for the study area analysis.

Figure 5 shows the relationship between different class areas over the years 1984, 1995, 2004, 2011, and 2019. Statistics show that the seawater area is up from 98095500 m² in 1984 to 109318500 m² in 2019. This means the eroded land is the difference between the two areas during this time. Therefore, during the period (1984-2019), green areas grew from 37519200 m² to 60516000 m². On the other hand, the coverage of Sabkha areas is increased slightly due to climate changes that have led to the rise of the sea level causing flooding.

TABLE 2
AREA OF DIFFERENT LAND COVER CLASSES OF CLASSIFIED IMAGES FOR DIFFERENT DATES 1984, 1995,2004, 2011, AND 2019.

Year	Urban area [m ²]	Green area [m ²]	Fish Bond [m ²]	Sea Water [m ²]	Sand [m ²]	Alluvial [m ²]	Sabkhas [m ²]
1984	4526100	37519200	0	98095500	24236100	55371510	14017590
1995	6261300	42597000	0	102943700	22974435	49582630	9406935
2004	8674200	58408300	0	106860500	13795740	36415620	9611640
2011	11693700	63340200	0	107529300	10894770	33447060	6860970
2019	12536100	60516000	11755147	109318500	13069553	15847200	10723500

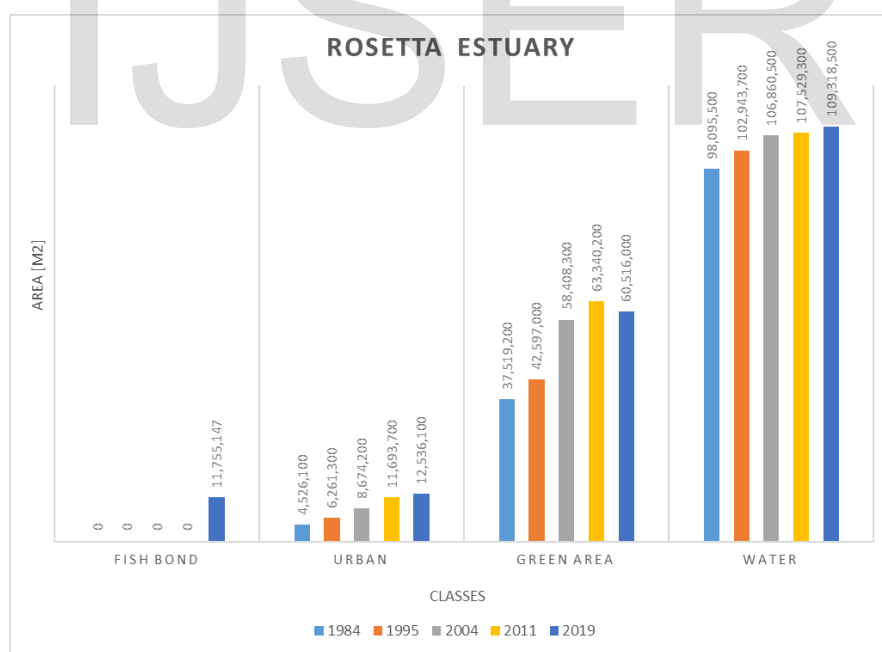


Fig. 5. Relationship between areas for different classes through the years 1984, 1995, 2004, 2011, and 2019.

4 DSAS RESULTS

4.1 DSAS software uncertainty

Firstly, an error between the measured and calculated shoreline position from DSAS software for the year 2019 is

computed and the predicted shoreline in the same year (Fig. 6), then we used this error to correct the predicted shorelines in years 2050 & 2100.

4.2 Qualitative analysis by DSAS from 1984 to 2019

4.2.1 Transects between years 1984 & 2019

Firstly, transects, between the years 1984, and 2019 were established using the LRR method as shown in Fig. 7. The figure shows the annual rates of shoreline changes. Fig. 8 shows the net area represented in erosion/ accretion patterns for the shorelines between the years 1984 and 2019. It is clear that

severe erosion dominates the Rosetta coastline due to lack of sediment and water discharged to the Mediterranean Sea in combination with constructing hard protection measures caused instability in the sediment budget at the study area.

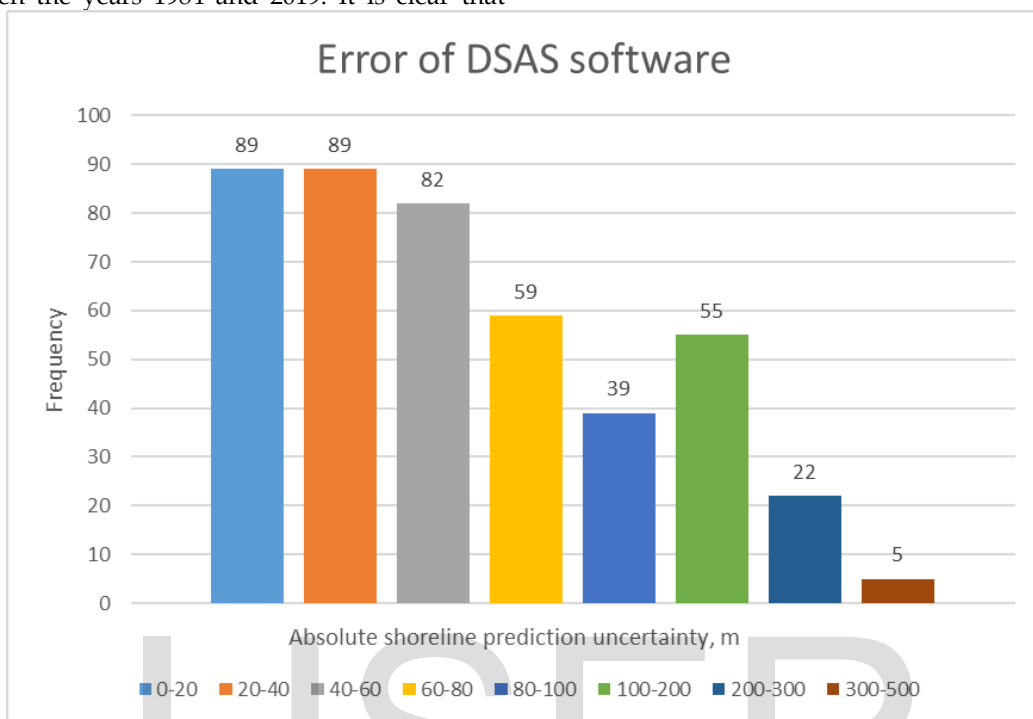


Fig. 6 DSAS Software uncertainty.

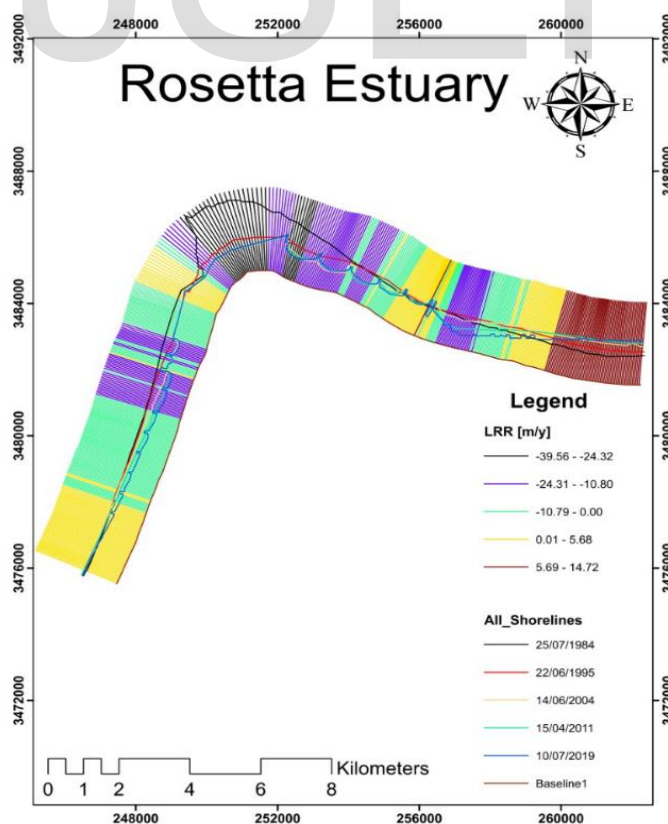


Fig. 7 Transects & shorelines from 1984 to 2019.

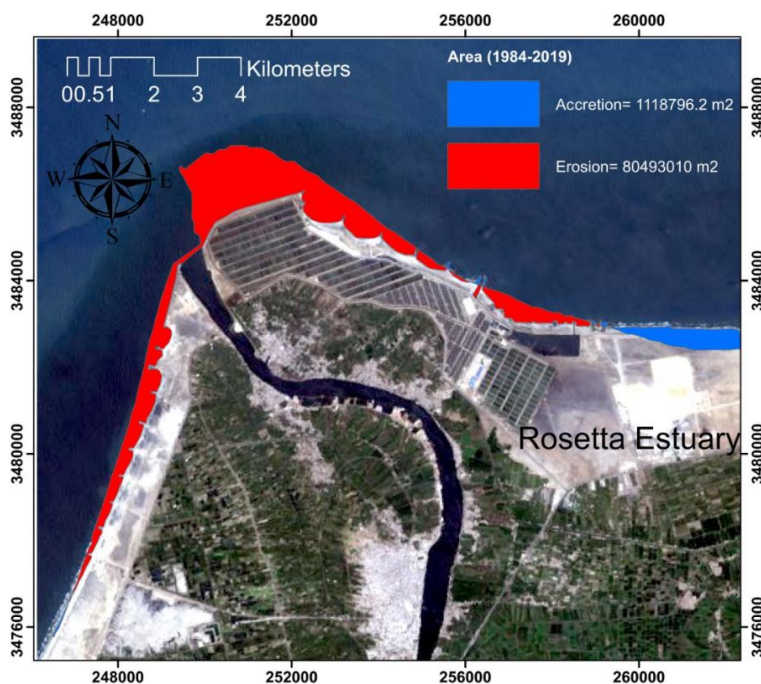


Fig. 8 Net area between the years 1984 & 2019.

The casted transects accompanied with (erosion/accretion) patterns resulted from detecting changes mechanism for different periods (1984-1995), (1995-2004), (2004-2011), and (2011-2019) are shown respectively from Figs 9 to 16. It is noticeable for the period (1984-1995) that erosion rate was severe particularly in front of the promontory at the eastern side (127 m/year) and decreased at the western one, while the accretion

extends downdrift due to the longshore currents driven by the dominant wave from NW direction. During the period (1995-2004), erosion continues creeping towards land until it reaches the seawalls constructed in front of the promontory at both sides, and the erosion rate decreased slightly to be about 45 m/year.

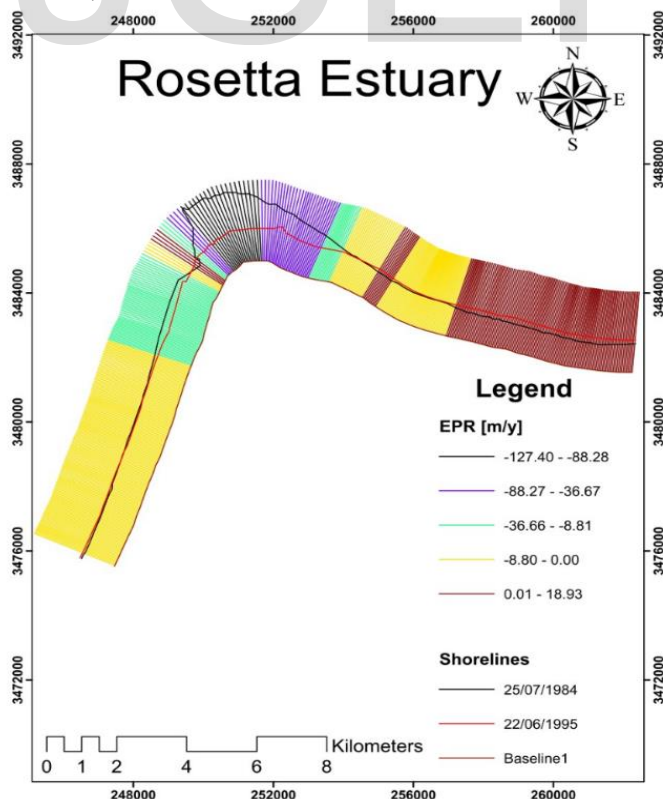


Fig. 9. Transects & shorelines from 1984 to 1995.

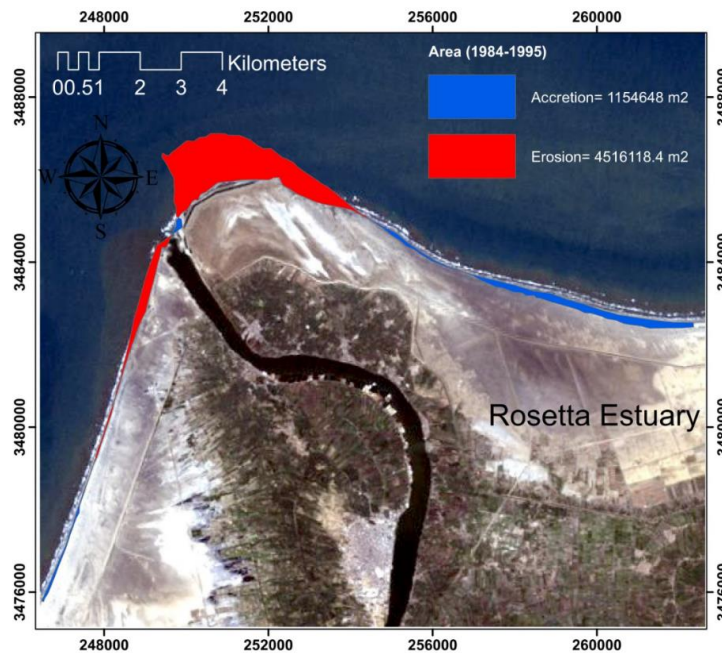


Fig. 10 Net areas between the years 1984 & 1995.

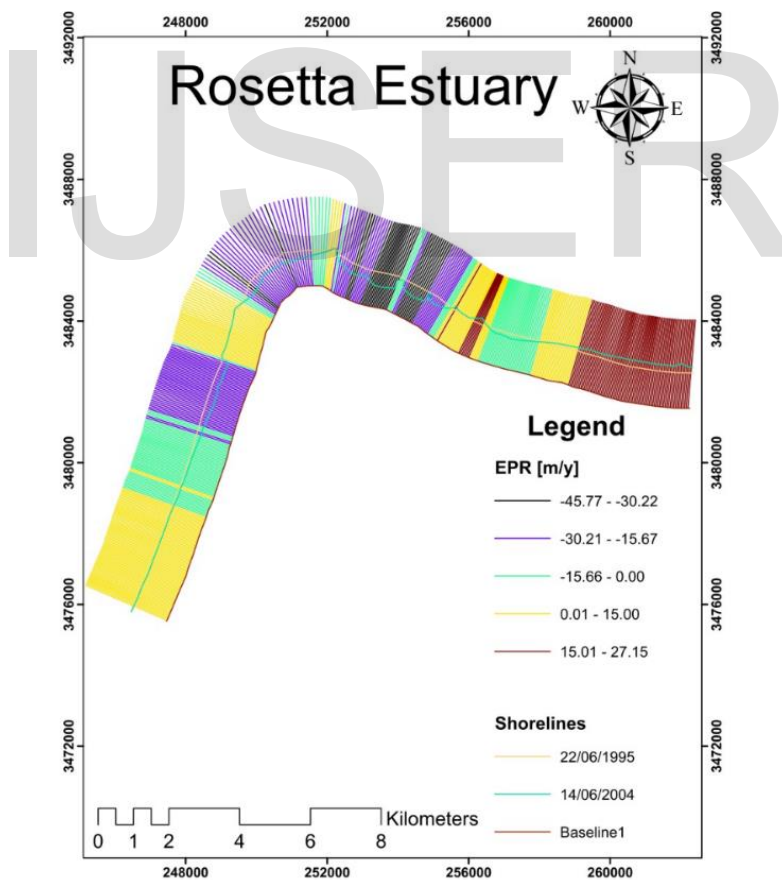


Fig. 11 Transects & shorelines from 1995 to 2004.

During the period (2004-2011), erosion has been stopped at front of seawalls, and redirected to the downdrift specifically, the eastern side passing the groins (built to decrease erosion). The maximum erosion rate was 45 m/year at the eastern side

of the promontory. During the period (2011-2019), the erosion rate slightly increased to be 59 m/year. However, the erosion will continue as the human-made modification occurred due to interference with the natural stability of the promontory.

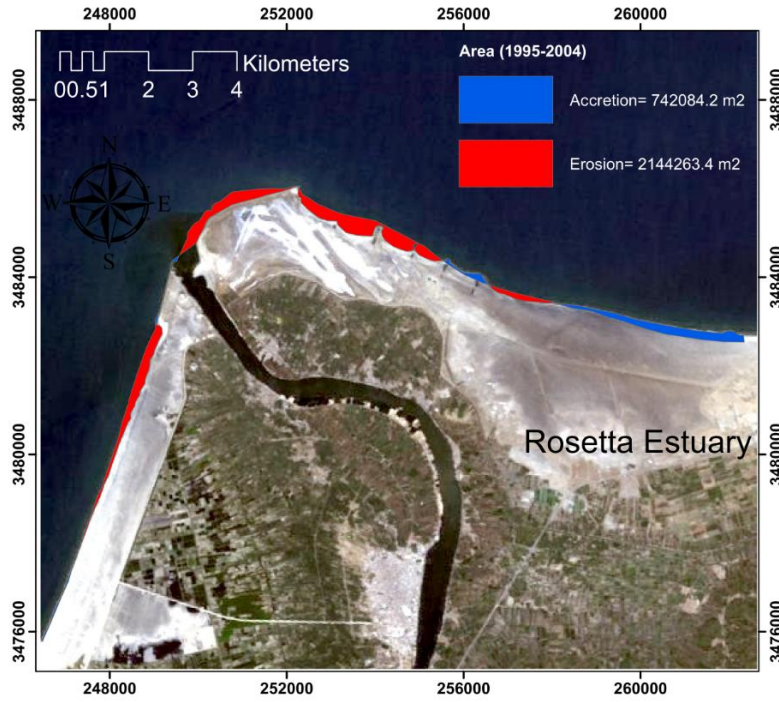


Fig. 12 The net area between the years 1995 & 2004.

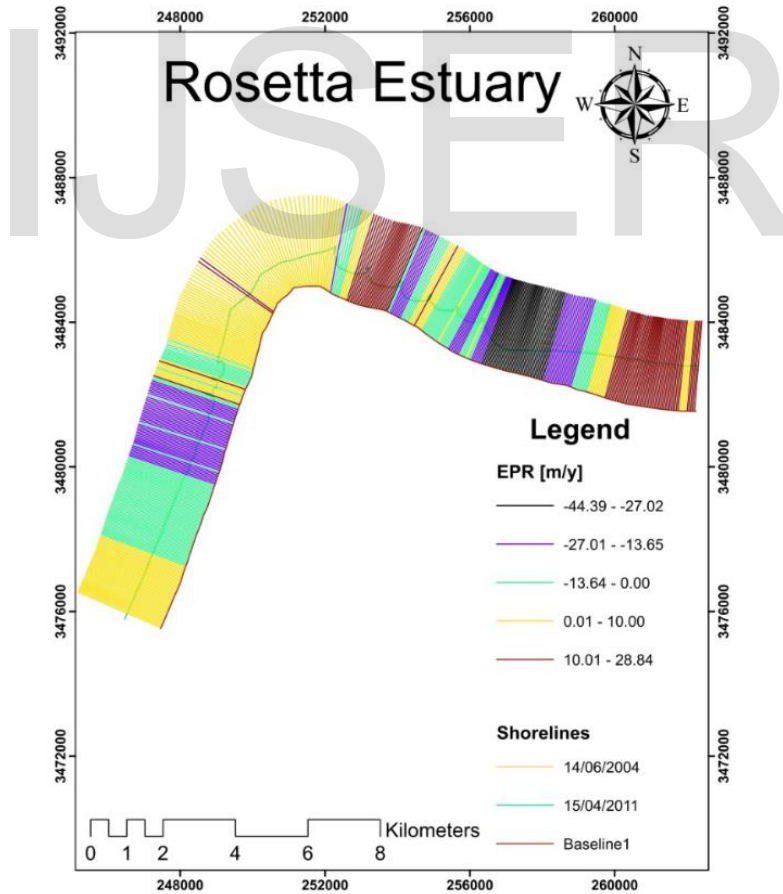


Fig. 13 Transects & shorelines from 2004 to 2011.

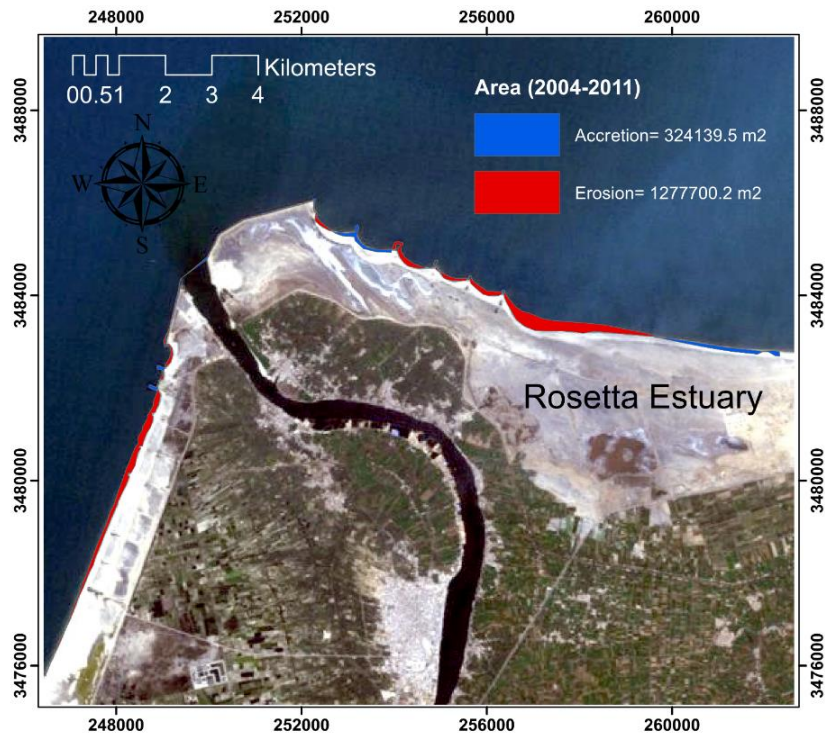


Fig. 14 Net areas between the years 2004 to 2011.

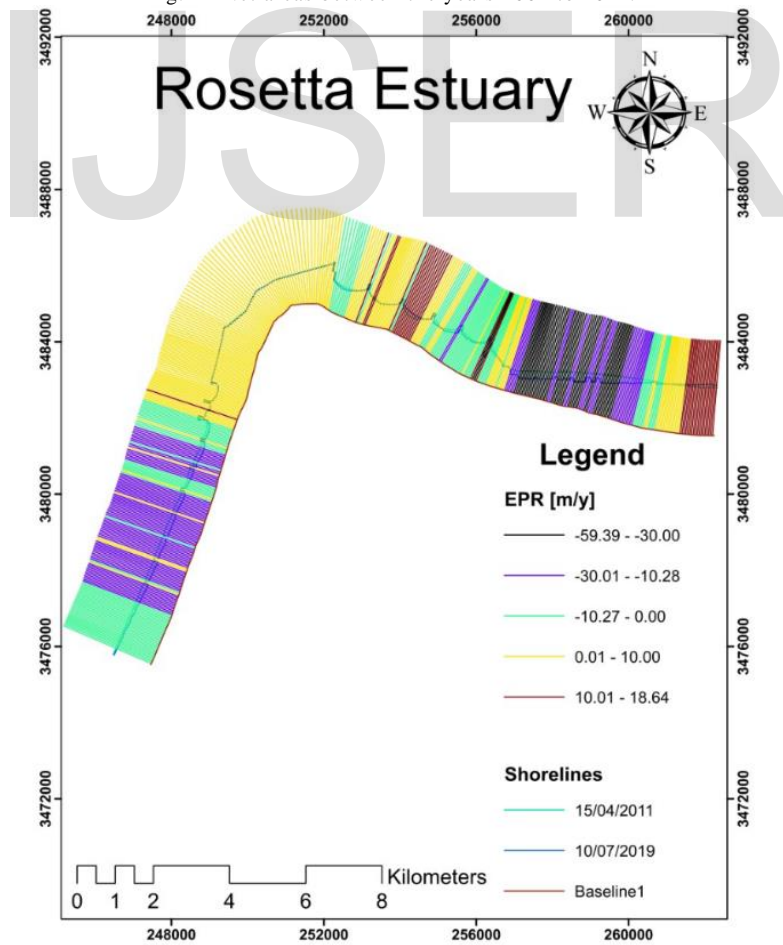


Fig. 15 Transects & shorelines from 2011 to 2019.

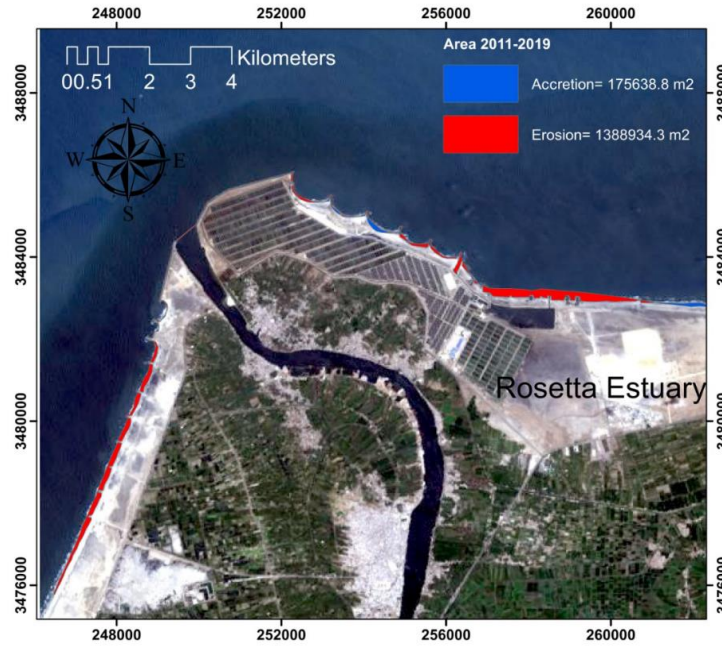


Fig. 16 The net area between the years 2011 to 2019.

4.3 Prediction by DSAS from (2019 to 2100)

In this section, the accretion/erosion rates by DSAS have been predicted, (Fig. 17), besides identifying erosion/accretion patterns through ARCGIS software between (2019-2040), (2040-2070), and (2070-2100), (Figs. 18 to 21). It is remarked that the

erosion rate from (2019-2100) will not rapidly rise as forecasted before. The erosion rate is predicted to be 28 m/year and this attribute to the study area nearly reaches the stability as the erosion will extend to distances far away from it at downdrift.

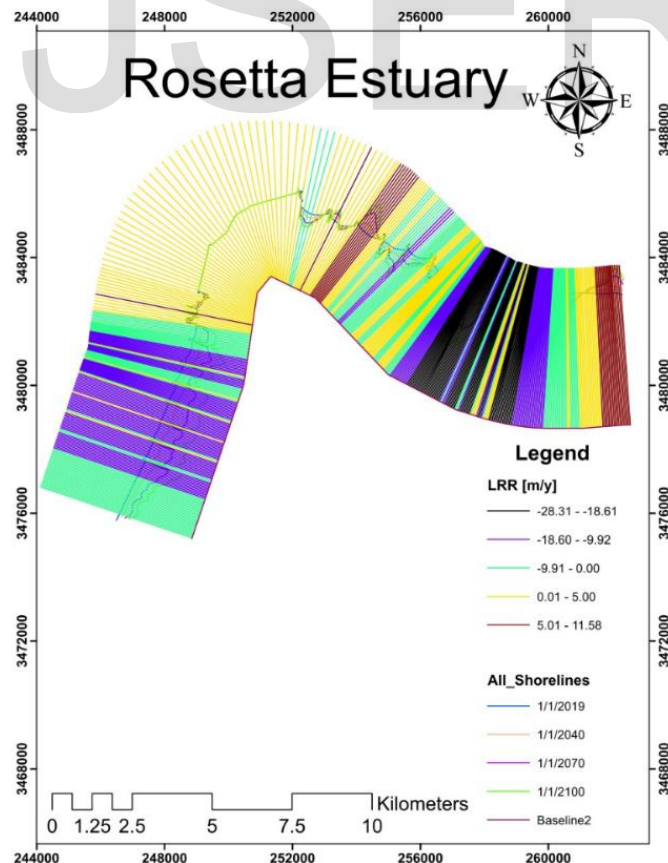


Fig. 17 Transects & shorelines from 2019 to 2100.

4.3.1 The area between the years 2070 & 2100

As a result of the prediction of the shoreline from 2070 until 2100, there was accretion and erosion in the areas of Rosetta promontory.

4.3.2 The area between the years 2019 & 2040

As a result of the prediction of the shoreline from 2019 until 2040, there was accretion and erosion in the areas of Rosetta promontory.

4.3.3 The area between the years 2040 & 2070

As a result of the prediction of the shoreline from 2040 until 2070, there was accretion and erosion in the areas of Rosetta promontory.

4.3.4 The area between the years 2019 & 2100

As a result of the prediction of the shoreline from 2019 until 2100, there was accretion and erosion in the areas of Rosetta promontory.

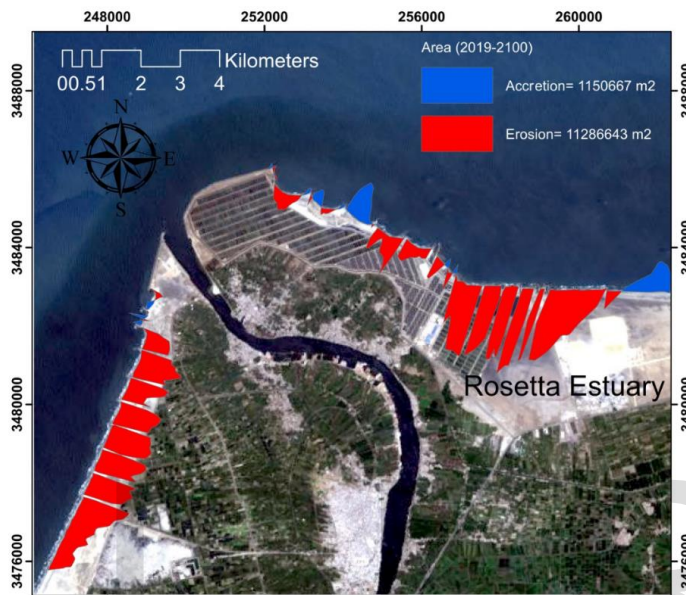


Fig. 18 The net area between the years 2019 & 2100.

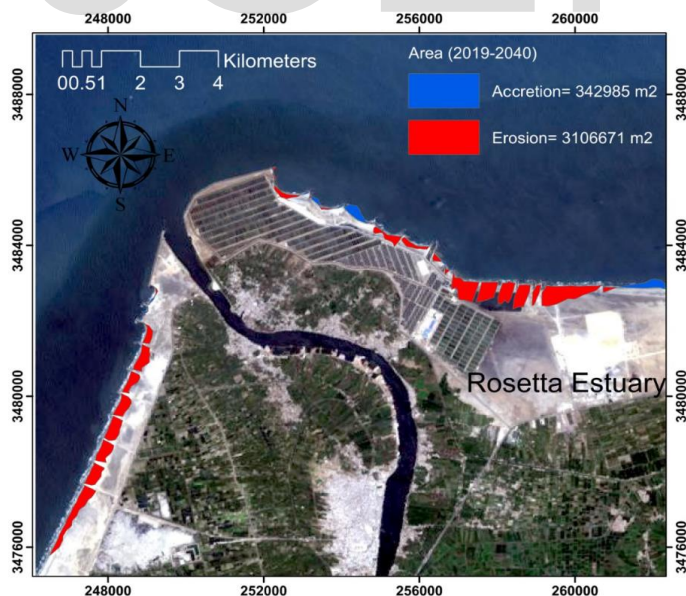


Fig. 19 The net area between the years 2019 & 2040.

It is clear from Figs. 22 and 23 that the maximum erosion rate was confined in front of the eastern side during the period (1984-2019) almost all the time, while after 2019 to 2100, it is predicted that the maximum eroding rate happened at the downdrift of the eastern groins. Table 3 indicates the annual

erosion rate and the expected one. However, the situation in front of seawalls at the eastern and western sides will be exacerbated if there is no periodic maintenance to the seawalls as the local erosion in front of it forms a great threat and may lead it to failure.

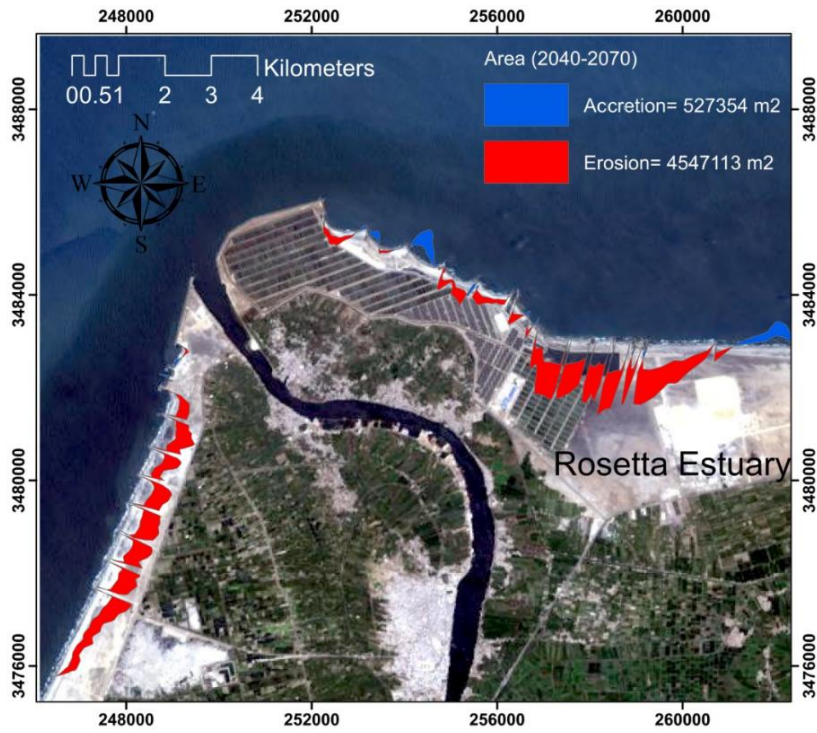


Fig. 20 The net area between the years 2040 & 2070.

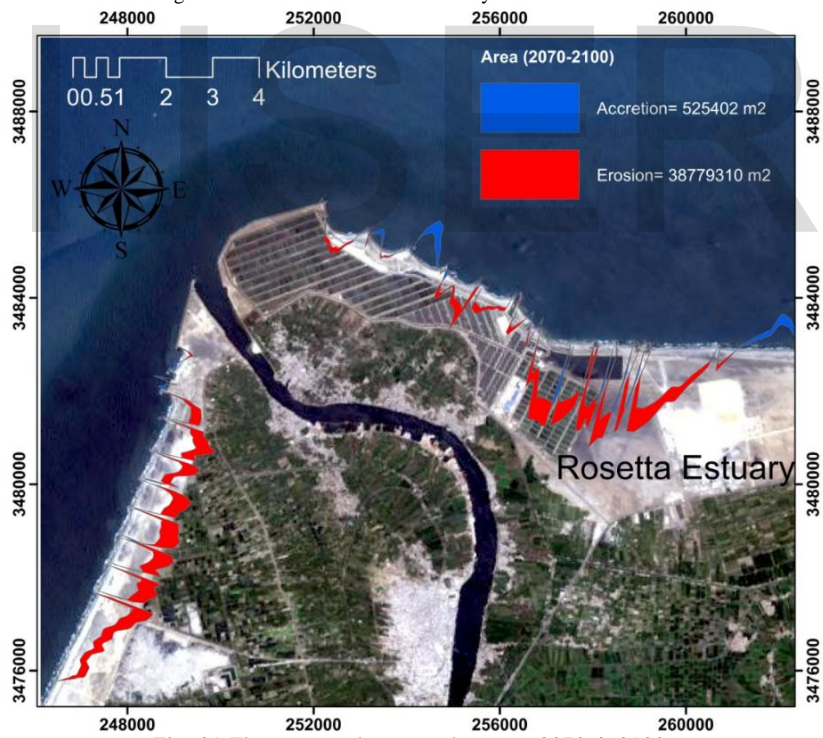


Fig. 21 The net area between the years 2070 & 2100.

TABLE 3
 The relationship between LRR (Mean) & Evaluation and years.

Year	LRR (Mean)	Evaluation
(1984-2019)	-6.4 m	Erosion
(2019-2100)	- 7.8 m	Erosion

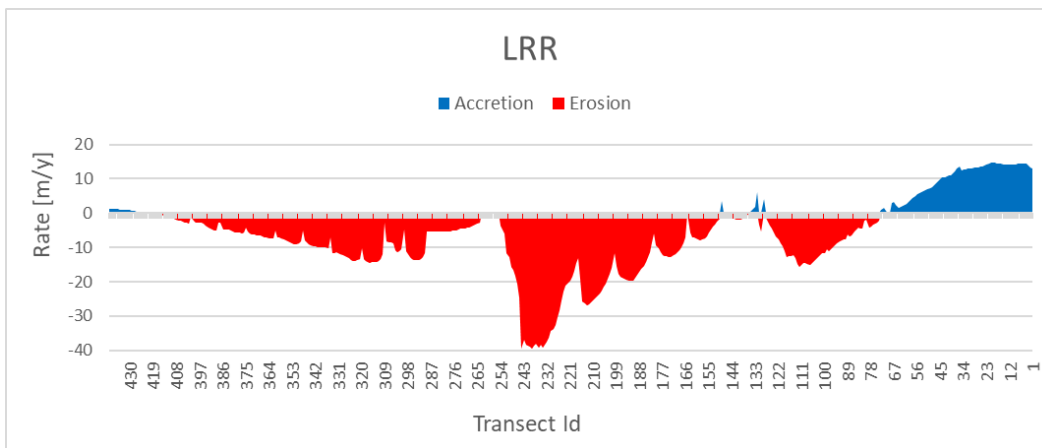


Fig. 22 Erosion/accretion rates using LRR technique from 1984 to 2019.

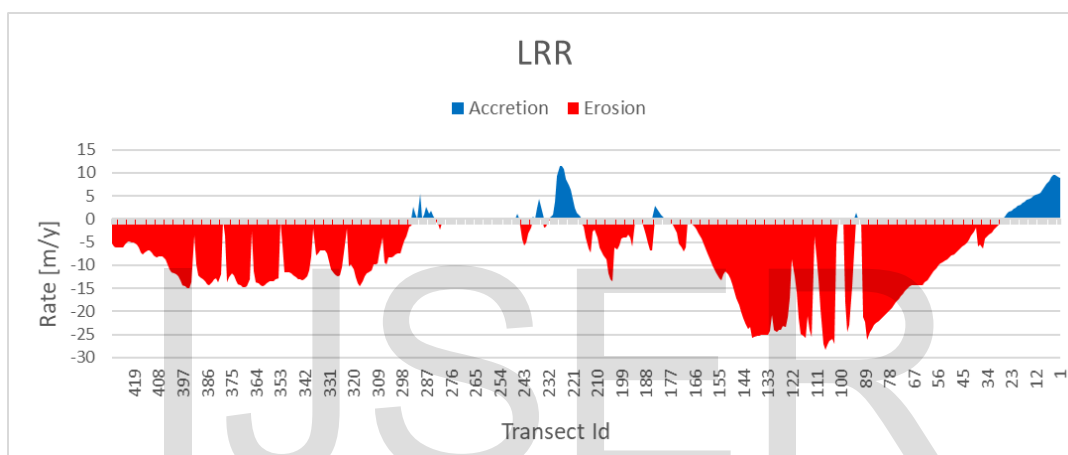


Fig. 23 Erosion/accretion rates using LRR technique from 2019 to 2100.

5 Decision Matrix

A decision matrix is considered a simple tool, especially when there are many alternatives and criteria of diverse significance, which is useful in making decisions that are complex. Table 4 displays the recently introduced EPR- and LRR-based shoreline classification. Moreover, the methodology of the decision algorithm is performed by (Karim Nassar et al. 2018). The final decision is made on the basis of the sub-regions divided into a cluster of areas (Tables. 5 and 6). The first is based on erosion and accretion severity (Table 4). The second evaluation, however, included a level of risk of near-shore erosion

and sedimentation hazard services that Mahapatra et al. (2015) and Frihy & EL-Sayed (2013) had virtually previously studied because the sensitivity to risk was classified as high, moderate and low. This category was analyzed on the basis of possible socio-environmental losses resulting from coastal erosion and programming by the surrounding coastal services. A maximum-likelihood controlled classification of land cover for each area is achieved in this research. According to this classification, the risk index is established by Mahapatra et al. (2015) for each sub-region based on the land-use coefficient.

TABLE 4
Classification of shoreline based on EPR, and LRR (Karim Nassar et al. 2018).

Category	shoreline change rate (m/year)	classification of shoreline
1	> -2	Very high erosion
2	> -1 and < -2	High erosion
3	> 0 and < -1	Moderate eroding
4	0	Stable
5	> 0 and < +1	Moderate accretion
6	> +1 and < +2	High accretion
7	> +2	Very high accretion

TABLE 5
Decision matrix indicating shoreline evolution and risk assessment between 1984 and 2019 by LRR

Rosetta Estuary		Rate of Change, LRR (m/y)	Sector Name	Length (km)	Transect Id & NO. of transects	Mean LRR (m/y)	Evaluation	Risk Level	Decision (Artificial Protection)
	LRR		A	8	(265-424) 160 Transect	-6.95	Very High erosion	High	-----
	LRR		B	6,15	(132-254) 123 Transect	-16.4	Very High erosion		-----
	LRR		C	2,9	(74-131) 58 Transect	-8.31	Very High erosion		-----
	LRR		D	3,65	(1-73) 73 Transect	+9.815	Very High accretion		-----
	LRR		-	20,7	414	-6.4	-		-----

During the time (1984–2019), the matrix was generated on the basis of LRR as shown in Table 5. Rosetta zone is composed of four sequential sub-areas (i.e. A, B, C, and D) by the erosion/accretion rate curve concavity shifts as outputs from LRR. The coastal extension of Rosetta from west to east, along with a combination of LRR feature class and transect class in ArcMap 10.2.2, is marked by a quantified multimedia erosion/accretion transect map. The recession shorelines are situated in sectors A, B and C, while the shorelines are accreted in sectors D. In Sector B center there is a maximum eroding rate of -16,4 m /year. Then, the coastal drifts crawl eastward along the coast of Rosetta powered by eastward currents to the D sector at a maximum accretion rate of +9,815 m / year.

In addition, for the adjusted shorelines between 2019 and 2100, the foreseeable fluctuations of LRR from west to east along the coastline of Rosetta, using 5 sectors A, B, C, D, and E, are calculated and graphically tracked in Table 6. Indeed, a strong correspondence is observed between future-oriented and historical LRR trends, which means that the predictions almost follow the same eroding and accretion activity. In addition, the forecast shoreline of the LRR model shows that the maximum eroding in sector D will be -11,6 m / year. The continuation of this rate in this region will result in a complete collapse of the Rosetta estuary ecosystem by 2100. In addition, the highlighted red sectors mean that approximately 90% of Rosetta's coastline is very vulnerable to degradation. In these areas, immediate measures are therefore necessary to decrease

the erosion rate.

According to the above two mentioned tables, the degree of vulnerability is categorized as follows:

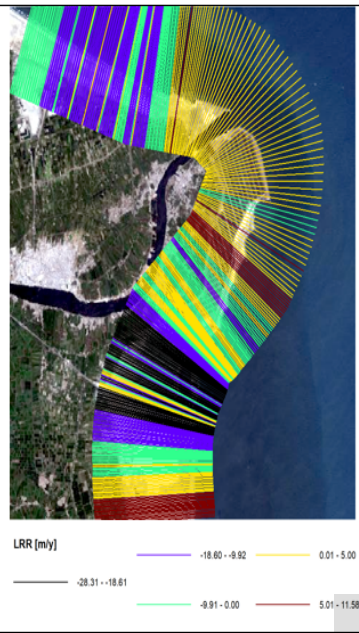
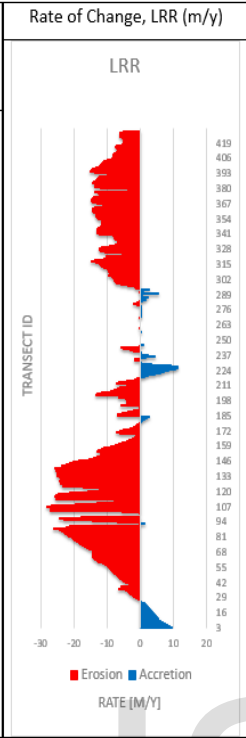
Zone (A): Very high erosion, high risk, required artificial protection with sand nourishment along 6.8 Km.

Zone (D): Very high erosion, high risk, required artificial protection with sand nourishment along 9.55 Km.

6 CONCLUSION

Shoreline changes along the Rosetta coast from 1984 to 2019 are easily discovered and computed through geospatial techniques and automatic calculations done by DSAS. Firstly, supervised classification has been applied to the study area using several Landsat images to detect the changes. It is clear that severe erosion occurred in almost the whole area. Besides Accretion/Erosion patterns have been mapped through the period (1984-2019). Moreover, Shoreline change rates have been mapped along the shoreline using DSAS software which extracts valuable information regarding erosion pattern, erosion rates, and its specific location. Finally, a decision matrix has been developed to identify the degree of vulnerability along the shoreline of Rosetta. This tool proved to be a valuable tool for decision-makers. This study provides local coastal managers and decision-makers with a highly reliable tool of decision support that may help in evaluating coastal changes to elaborate coastal management plans in Rosetta Promontory.

TABLE 6
Decision prediction matrix indicating shoreline evolution and risk assessment between 2019 and 2100 by LRR

Rosetta Estuary		Rate of Change, LRR (m/y)		Sector Name	Length (km)	Transect Id & NO. of transects	Mean LRR (m/y)	Evaluation	Risk Level	Decision (Artificial Protection)
		A	6,8	(294-429) 136 Transect	-9.9	Very High Erosion	High	Protection Required		
		B	2,35	(247-293) 47 Transect	~ 0.00	Almost Stable		Protection not Required		
		C	1,45	(218-246) 29 Transect	+2.25	Very High Accretion		Protection required		
		D	9,55	(27-217) 191 Transect	-11.6	Very High Erosion		Protection not required		
		E	1,3	(1-26) 26 Transect	+5.1	Very High Accretion		-		
		-	21,45	429	-7.8	-		-		

ACKNOWLEDGMENT

A special and sincere word of thanks is extended to all my supervisors for their kind help, encouragement, and valuable suggestions. Their kind guidance is deeply appreciated. Special thanks go to Dr. Karim Nassar for his great help.

REFERENCES

[1] Addo, K.A. & Kufogbe, K.S., 2011. Quantitative Analysis of Shoreline Change Using Medium Resolution Satellite Imagery in Keta , Ghana. , 1(1), pp.1-9.

[2] Ahmed, A.S.M., 2006. Numerical model as a tool to investigate coastal problems in Egypt. In *Tenth International Water Technology Conference, IWTC10*. pp. 933-944.

[3] Anand, R., Chandrasekar, B.N. & Magesh, S.K.N.S., 2016. Shoreline change rate and erosion risk assessment along the Trou Aux Biches - Mont Choisy beach on the northwest coast of Mauritius using GIS-DSAS technique. *Environmental Earth Sciences*, 75(5), pp.1-12.

[4] Badr, A.M.A., Abdella, F.A. & El-kolfat, A.I., 2005. Coastal changes along Rosetta promontory. *Alexandria Engineering Journal*, 44(1), pp.91-100.

[5] Elsayed, M.A.K. et al., 2005. Accretion and erosion patterns along Rosetta promontory, Nile Delta coast. *Journal of Coastal Research*, 21(3), pp.412-420.

[6] El-sharnouby, B.A. et al., 2015. Coastal Changes along Gamasa Beach , Egypt. , 17(2).

[7] Fanos, A.M., 2001. Nile Delta Coastal Zone. International workshop on the Planning and Management of Modified Major Deltas, 24-26th September , Netherlands.

[8] Fanos, A.M., Naffaa, M.G., et al., 1995. Seasonally and yearly wave regime and climate of the Mediterranean coast of Egypt. In *COPEDEC IV, Rio de Janeiro, Brazil*.

[9] Fanos, A.M., Khafagy, A.A. & Dean, R.G., 1995. Protective works on the Nile Delta coast. *Journal of Coastal Research*, 11(2), pp.516-528.

[10] Frihy, O. et al., 1994. Remote sensing of beach erosion along the Rosetta promontory, northwestern Nile delta, Egypt. *International Journal of Remote Sensing*, 15(8), pp.1649-1660.

[11] Frihy, O.E., 2001. The necessity of environmental impact assessment (EIA) in implementing coastal projects: lessons learned from the Egyptian Mediterranean Coast. *Ocean & Coastal Management*, 44(7-8), pp.489-516.

[12] Kabuth, A.K. et al., 2013. Multidecadal Shoreline Changes in Denmark Multidecadal Shoreline Changes in Denmark. , 30(4), pp.714-728.

- [13] Kermani, S. et al., 2016. Ocean & Coastal Management Detection and analysis of shoreline changes using geospatial tools and automatic computation: Case of jijelian sandy coast (East Algeria). *Ocean and Coastal Management*, 132, pp.46-58.
- [14] Masria, A. et al., 2015. Detection of Shoreline and Land Cover Changes around Rosetta Promontory, Egypt, Based on Remote Sensing Analysis. , pp.216-230.
- [15] Murali, R.M. et al., 2015. Decadal shoreline assessment using remote sensing along the central Odisha coast , India. , 74(10).
- [16] Naffaa, M.G., 1995. Wave Climate along the Nile Delta Coast. *Journal of Coastal Research*, 11(1), pp.219-229.
- [17] Nandi, S. et al., 2016. Shoreline shifting and its prediction using remote sensing and GIS techniques : a case study of Sagar Island , West Bengal (India). , pp.61-80.
- [18] Nassar, K., Fath, H., et al., 2018. Automatic detection of shoreline change: case of North Sinai coast, Egypt. *Journal of Coastal Conservation*.
- [19] Nassar, K., Mahmud, W.E., Masria, A., et al., 2018. Numerical simulation of shoreline responses in the vicinity of the western artificial inlet of the Bardawil Lagoon, Sinai Peninsula, Egypt. *Applied Ocean Research*, 74.
- [20] Nassar, K. et al., 2018. Shoreline change detection using DSAS technique: Case of North Sinai coast, Egypt. *Marine Georesources & Geotechnology*, pp.1-15.
- [21] Sharaf El Din, S.H. et al., 1989. Extreme sea level values on the Egyptian Mediterranean coast for the next 50 years. In *International Seminar on Climatic Fluctuations and Water Management, Cairo*.
- [22] Stanley, D.J. & Warne, A.G., 1993. Nile Delta: recent geological evolution and human impact. *Science*, 260(5108), pp.628-634.
- [23] Thi, V.T. et al., 2014. Application of remote sensing and GIS for detection of long-term mangrove shoreline changes in Mui Ca Mau , Vietnam. , pp.3781-3795.